# Role of operating conditions in the catalyst deactivation in the in-line steam reforming of volatiles from biomass fast pyrolysis

Aitor Arregi, Gartzen Lopez, Maider Amutio, Maite Artetxe, Itsaso Barbarias, Javier Bilbao and Martin Olazar

Department of Chemical Engineering, University of the Basque Country UPV/EHU, P.O. Box 644 - E48080 Bilbao (Spain). gartzen.lopez@ehu.eus

## Abstract

The effect of reforming conditions (temperature, space time and steam/biomass ratio (S/B)) has been studied in the continuous biomass pyrolysis and in-line catalytic steam reforming process in order to establish suitable conditions for attenuating the deactivation of a commercial Ni catalyst by coke deposition. The experiments have been performed in a conical spouted bed and a fluidized bed reactor for the pyrolysis and reforming steps, respectively. Biomass fast pyrolysis was performed at 500 ºC and the reforming operating conditions studied are as follows: 550-700 ºC; space-time, 10-30 $g_{catalyst}$ min $g_{volatiles}^{-1}$, and; S/B ratio, 2-5. The coke deposited on the catalyst has been analyzed by temperature programmed oxidation (TPO), and two types of coke have been identified, i.e., the coke deposited on the Ni active sites and the one separated from these sites, without filamentous coke being observed by transmission electron microscopy (TEM). Coke deposition has been related to the decomposition of the oxygenates derived from biomass pyrolysis and the re-polymerization of phenolic oxygenates. Suitable conditions to achieve almost full conversion with a $H_2$ yield of up to 95 % and stability for 160 min on stream, the following have been established: 600 ºC, space time of 30 $g_{catalyst}$ min $g_{volatiles}^{-1}$ and S/B ratio of 3.

**Keywords:** biomass; pyrolysis; reforming; hydrogen; deactivation; bio-oil

## 1. Introduction

Renewable fuels have attracted significant interest over the last years due to the environmental problems related to the massive use of petroleum based fuels, such as global warming and climate change [1]. In this scenario, biomass is considered one of the most important renewable raw materials with virtually no net contribution to global

greenhouse gas [2]. Thermochemical routes (such as gasification and fast pyrolysis) are regarded as the best strategies in terms of their scalability for conversion of biomass into bio-fuels [3]. High bio-oil yields can be obtained at moderate temperatures (around 500 ºC) from different types of biomasses and in a delocalized way by using simple design fast pyrolysis technologies [4,5].

Amongst the different alternatives for bio-oil valorization, steam reforming has received increasing attention for sustainable $H_2$ production [6-8]. The main interest of this process lies in its contribution to attenuating the current $CO_2$ emissions (produced from $CH_4$ reforming). Moreover, the bio-oil dehydration step, which is required for its valorization as fuel, is not needed for reforming. Nevertheless, several challenges should be faced to avoid bio-oil handling problems in the reforming process [9,10]. Thus, in order to avoid these problems and those related to bio-oil storage, the capability of pyrolysis-reforming of biomass for $H_2$ production has been recently proven by several authors [11-14] by combining two in-line reactors for biomass fast pyrolysis and the subsequent reforming of volatiles, which allow obtaining a $H_2$-rich gaseous product.

In previous papers, the good behaviour of the pyrolysis-reforming process by means of a conical spouted bed reactor (CSBR) and an in-line fluidized bed reactor (FBR) has been verified for different feeds, such as biomass [13], high density polyethylene (HDPE) [15], polystyrene (PS) [16] and biomass/HDPE mixtures [17]. In these studies, the performance of the CSBR is proven for pyrolysis of irregular texture or/and sticky materials, specifically for biomass [18-20]. Besides, the FBR is a suitable reactor for reforming, as it allows attaining a homogeneous temperature and attenuating operational problems reported in the literature for fixed bed reactors due to the high amount of coke deposited on the catalyst [21].

Nevertheless, the deactivation of the catalyst is a determining factor for its selection, reactor design, establishment of the optimum operating strategy and viability of pyrolysis-reforming of biomass when scaling up. Although pyrolysis-reforming studies dealing with the characterization of deactivated catalysts are very scarce in the literature, it is well-established that coke deposition is the main deactivation cause of Ni based catalysts [22-25]. The deactivation rate is a consequence of coke formation and gasification rates, which are influenced by reaction conditions [26,27].

The aim of this study is to investigate the effect reforming temperature, space time and steam/biomass (S/B) ratio have on the reforming products and especially, on catalyst deactivation, with the purpose of establishing suitable conditions for attenuating this problem. Moreover, coke content and type have been determined by temperature programmed oxidation (TPO) and transmission electron microscopy (TEM), in order to understand the role of coke in catalyst deactivation.

## 2. Experimental

### 2.1. Materials

Table 1 shows the properties of the pine wood sawdust used in this study (particle size in the 1-2 mm range), which have been determined by ultimate and proximate analyses by means of a LECO CHNS-932 elemental analyzer and a TGA Q5000IR thermogravimetric analyzer, respectively. Moreover, a Parr 1356 isoperibolic bomb calorimeter has been used for the measurement of the higher heating value (HHV).

**Table 1.** Properties of the pine wood sawdust used in the study.

| | |
|---|---|
| **Ultimate analysis (wt %)** | |
| Carbon | 49.33 |
| Hydrogen | 6.06 |
| Nitrogen | 0.04 |
| Oxygen | 44.57 |
| **Proximate analysis (wt %)** | |
| Volatile matter | 73.4 |
| Fixed carbon | 16.7 |
| Ash | 0.5 |
| Moisture | 9.4 |
| **HHV (MJ $kg^{-1}$)** | 19.8 |

In addition, a commercial catalyst (G90-LDP) for $CH_4$ reforming has been used in the reforming step of biomass pyrolysis volatiles, which has been supplied by Süd Chemie (Germany) in the form of ribbed-rings having 10 hole ring shape and 19 x 16 mm size. Nevertheless, a particle size between 0.4 and 0.8 mm was required to attain a stable fluidization regime in the FBR, and therefore the catalyst had to be ground and sieved to

that particle size. The chemical formulation of the catalyst is based on NiO (nominal content of 14 wt %), $CaAl_2O_4$ and $Al_2O_3$. The results obtained by $N_2$ adsorption-desorption technique (Micromeritics ASAP 2010) have been reported in previous studies [21,28] and revealed a low BET surface area of the catalyst (19 $m^2$ $g^{-1}$) and an average pore diameter of 122 Å.

Moreover, the catalyst has been reduced in-situ by feeding a 10 vol % $H_2$ at 710 ºC for 4 h. The reduction temperature was determined by the results obtained in an AutoChem II 2920 Micromeritics by temperature programmed reduction (TPR), with the results being available in previous papers by the research group [21,28]. Two main peaks were observed at around 550 and 700 ºC, which were related to the reduction of NiO and $NiAl_2O_4$ phases, respectively.

## 2.2 Reaction equipment

The bench scale laboratory plant used for pyrolysis-reforming of biomass is provided with the following elements: pyrolysis reactor (conical spouted bed reactor, CSBR) and catalytic reforming reactor (fluidized bed reactor, FBR). These devices together with all interconnection pipes are located inside a forced convection oven in order to maintain the box temperature at 300 ºC and avoid the condensation of heavy compounds upstream and downstream the FBR, which in the latter case is essential to avoid the condensation of volatile products prior to their chromatographic analysis. The overall scheme of the plant is shown in Figure 1.

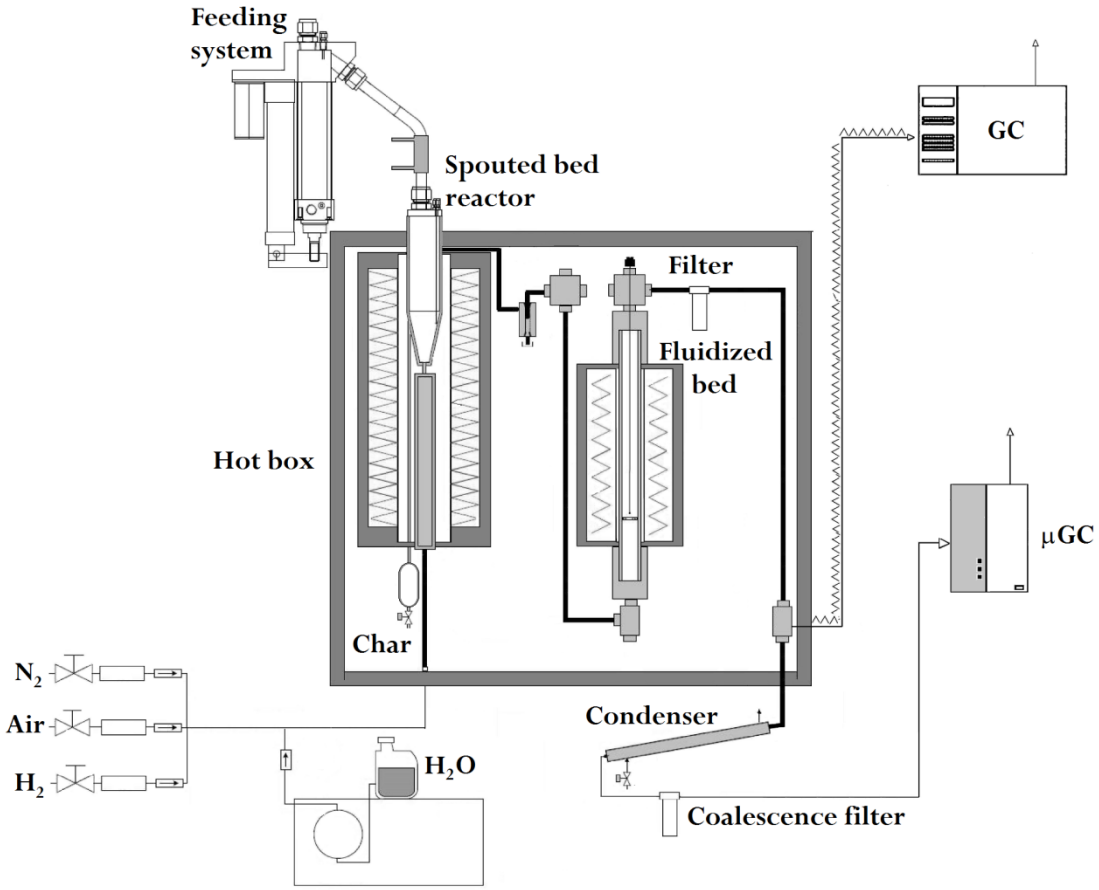


**Figure 1.** Scheme of the laboratory scale pyrolysis-reforming plant.

The CSBR has been previously used by the research group in the pyrolysis and gasification of biomass [18,20,29], plastics [30-32] and tyres [33,34] and has been designed with the following dimensions: height of the conical section, 73 mm; diameter of the cylindrical section, 60.3 mm, angle of the conical section, 30 º; diameter of the bed bottom, 12.5 mm, and; diameter of the gas inlet, 7.6 mm. Moreover, a gas preheater is located below the CSBR, which consists of a stainless steel cylindrical shell, with 31 mm in height and 27 mm in internal diameter. It is filled with stainless steel pipes that increase the surface area for heat transfer and heat the gases to the reaction temperature. Both the CSBR and gas preheater are located inside a 1250 W oven, which provides the heat required to reach the reaction temperature and preheat the gaseous stream to the reaction temperature. Moreover, the char formed is continuously removed from the pyrolysis reactor by means of a lateral outlet pipe to avoid its accumulation in the bed (see Figure 1).

A FBR with a length of 440 mm and an internal diameter of 38.1 mm has been used for the in-line catalytic reforming of biomass pyrolysis volatiles. The reactor is located inside a 550 W oven, and provides the heat required to maintain the reaction temperature, which is controlled by a thermocouple inside the catalyst bed.

The biomass feeding system consists of a cylindrical vessel equipped with a vertical shaft connected to a piston placed below the biomass bed. While the piston rises, the whole system vibrates and the feeding is discharged through a pipe cooled with tap water. A *Gilson 307* pump has been used to supply the reactor with water, which is vaporized prior to entering the gas preheater in a heating cartridge located inside the hot box.

Moreover, the pilot plant is provided with a solid-gas separation system equipped with a cyclone and a filter, in order to remove the char and sand particles entrained from the pyrolysis reactor and the small particles of the catalyst entrained by attrition in the reforming reactor, respectively. In addition, the liquid-gas separation system is provided with a condenser and a coalescence filter.

## 2.3 Product analysis

The in-line analysis of the volatiles derived from the reforming reactor has been carried out by means of a GC Agilent 6890, which is equipped with a HP-Pona column and a flame ionization detector (FID). A sample of the reforming reactor outlet stream (prior to condensation) has been injected into the gas chromatograph by means of a line thermostated at 280 ºC. On the other hand, the non-condensable gases ($H_2$, $CO_2$, CO, $CH_4$ and $C_2$-$C_4$ hydrocarbons) have been analyzed in-line in a micro GC Varian 4900, once the outlet stream of the reforming reactor has been condensed and filtered.

The coke content deposited on the catalyst has been studied at the end of the continuous runs by temperature programmed oxidation (TPO) in a thermobalance connected to a *Balzers Instruments Thermostar* mass spectrometer. Given that the Ni on the catalyst is oxidized together with the carbonaceous coke, this procedure allows monitoring $CO_2$ formation throughout the TPO runs. The procedure used is as follows: (i) signal stabilization with a He stream (10 mL $min^{-1}$) at 100 ºC, and (ii) oxidation with air (50 mL $min^{-1}$) following a ramp of 5 ºC $min^{-1}$ to 800 ºC, which has been kept for 30 min to

147 guarantee total coke combustion. In addition, the nature of the coke deposited has been
148 analyzed by transmission electron microscopy (TEM) images (Philips CM200).

149 2.4. Experimental conditions

150 In order to set suitable operating conditions in the pyrolysis step, the selected
151 temperature has been 500 ºC, given that below this temperature the biomass is not
152 completely degraded and above this one the liquid fraction (bio-oil) decreases [35].
153 Moreover, the steam flow rate and particle size of the sand in the conical spouted bed
154 reactor, and catalyst and sand particle sizes in the fluidized bed reactor, are conditioned
155 by fluid dynamic requirements in both reactors in-line, given that the former is spouted
156 and the latter fluidized with a common gas flow. Based on fluid dynamic runs in both
157 reactors, a water flow rate of 3 mL $min^{-1}$ has been established as suitable, which
158 corresponds to a steam flow of 3.73 NL $min^{-1}$, with 50 g of sand in the CSBR bed
159 (particle size in the 0.3-0.35 mm range) for attaining a vigorous movement. In the FBR,
160 the bed contains 25 g (mixture of catalyst and sand, with catalyst content being
161 established by space time), with the particle size of the catalyst and the sand being in the
162 0.4-0.8 mm and 0.3-0.35 mm ranges, respectively. The fluidization velocity is between
163 3 and 4 times the minimum one, which ensures both stable fluidization of the bed, even
164 when the catalyst has a high coke content, and moderate attrition of the catalyst.

165 In the steam reforming of biomass pyrolysis products, the effect of temperature has been
166 studied at 550, 600, 650 and 700 ºC, with a space time of 20 $g_{catalyst}$ min $g_{volatiles}^{-1}$ and a
167 S/B ratio of 4. It should be noted that a minimum reaction temperature of 550 ºC has
168 been established, given that below this temperature the conversion of biomass pyrolysis
169 volatiles is very low, which causes operational problems and high coke deposition on
170 the catalyst. The ceiling reaction temperature is conditioned by the reduction
171 temperature of the catalyst (710 ºC), so that higher temperatures lead to irreversible
172 deactivation of the catalyst by Ni sintering. Similarly, the effect of space time has been
173 studied between 2.5 and 30 $g_{catalyst}$ min $g_{volatiles}^{-1}$ at 600 ºC with a S/B ratio of 4. Finally,
174 the effect of S/B ratio has been studied in the 2-5 range (S/C ratios in the 3.9-9.7 range),
175 which has been attained by keeping the water flow rate at 3 mL $min^{-1}$ and varying the
176 amount of biomass fed into the process in the 0.6-1.5 g $min^{-1}$ range in order to ensure
177 suitable fluid dynamic conditions and maintain the same space time value.

178 2.5. Reaction indices

179 The conversion was determined as a percentage of the C units contained in the volatiles
180 fed into the reforming step that are recovered in the gaseous product (CO, $CO_2$, $CH_4$ and
181 $C_2$-$C_4$ hydrocarbons, mainly ethylene and ethane). The C content of the volatiles fed
182 into the reforming reactor has been determined based on the composition of the
183 pyrolysis outlet stream, so that the difference between the C content in the biomass and
184 in the pyrolysis outlet stream is the C contained in the char, which is removed from the
185 first reactor.

186 $$X(\%) = \frac{C_{gas}}{C_{volatiles}} 100 \quad (1)$$

187 The yields of C containing products have been quantified based on the flow rate of C
188 units in each product ($F_i$) and the flow rate of C units in the biomass pyrolysis volatile
189 stream ($F_{volatiles}$) fed into the reforming reactor.

190 $$Y_i(\%) = \frac{F_i}{F_{volatiles}} 100 \quad (2)$$

191 In addition, $H_2$ yield is stated as a percentage of the maximum allowable by
192 stoichiometry, considering all oxygenated compounds are converted into $H_2$ and $CO_2$.

193 $$Y_{H_2}(\%) = \frac{F_{H_2}}{F_{H_2}^0} 100 \quad (3)$$

194 where $F_{H2}$ is the molar flow rate of $H_2$ produced in the reforming step and $F_{H2}^0$ the
195 maximum molar flow rate allowable by stoichiometry:

196 $$C_n H_m O_k + (2n-k) H_2O \rightarrow nCO_2 + (2n + m/2 - k) H_2 \quad (4)$$

197 Finally, $H_2$ production is defined by mass unit of the biomass in the feed into the
198 pyrolysis-reforming system, and has been calculated as follows:

199 $$P_{H_2}(wt\ \%) = \frac{m_{H_2}}{m_0} 100 \quad (5)$$

where $m_{H2}$ and $m_0$ are the mass flow rates of the $H_2$ produced and the biomass fed into the system, respectively.

## 3. Results

A study has been carried out on the effect reforming conditions (temperature, space time and S/B ratio) have on conversion, product yields and catalyst deactivation. All experiments have been performed using a pyrolysis temperature of 500 ºC, given that the production of oxygenated volatiles is maximized at this temperature in the CSBR [35]. A temperature between 500 and 600 ºC has also been used by other authors in the pyrolysis step, with pine wood in the feed [22,36-39]. Moreover, a comparison between biomass pyrolysis with $N_2$ and steam has been carried out in a previous paper, with the effect of the fluidizing agent ($N_2$ or steam) on product distribution being insignificant due to the relatively low temperature (500 ºC) and short residence time of the volatiles in the CSBR [13]. Thus, 75 wt % of bio-oil, 8 wt % of gases and 17 wt % of char are obtained in the biomass pyrolysis in a CSBR. The bio-oil contains water (25 wt %) and a mixture of different oxygenated compounds, with the main products being phenols (16.5 wt %), ketones (6.4 wt %), saccharides (4.5 wt %), furans (3.3 wt %), acids (2.7 wt %), alcohols (2.0 wt %) and aldehydes (1.9 wt %). Moreover, the gas fraction is mainly made up of CO (3.4 wt %), $CO_2$ (3.3 wt %) and a low concentration of $CH_4$ (0.4 wt %), $C_2$-$C_4$ hydrocarbons (0.3 wt %) and $H_2$ (0.004 wt %). Consequently, the composition of the volatiles fed into the reforming step is the one corresponding to this stream and the reforming steam flow rate.

Furthermore, in order to explain the product distributions obtained, the following reactions have been considered in the reforming step: steam reforming of oxygenated compounds (eq. 6), $CH_4$ (eq. 7) and $C_2$-$C_4$ hydrocarbons (eq. 8), water gas shift (WGS) reaction (eq. 9) and decomposition/cracking of oxygenated compounds (eq. 10), with the latter being one of the reactions responsible for coke formation.

$$C_nH_mO_k + (n-k)H_2O \rightarrow nCO + (n+m/2-k)H_2 \quad (6)$$

$$CH_4 + H_2O \leftrightarrow CO + 3H_2 \quad (7)$$

$$C_rH_s + rH_2O \rightarrow rCO + (r+s/2)H_2 \quad (8)$$

229 $$CO + H_2O \leftrightarrow CO_2 + H_2 \quad (9)$$

230 $$C_nH_mO_k \rightarrow C_xH_yO_z + C_rC_s + CH_4 + CO + CO_2 + C(coke) \quad (10)$$

231 3.1. Effect of reforming temperature

232 The effect of temperature on catalyst deactivation has been studied between 550 and
233 700 ºC, and all the results have been obtained with a space time of 20 $g_{catalyst}$ min
234 $g_{volatiles}^{-1}$ and a S/B ratio of 4. As observed in Figure 2, at 550 ºC the conversion
235 obtained at zero time on stream is low (< 60 %), whereas above 600 ºC almost full
236 conversion is achieved under these conditions, in which thermodynamic equilibrium is
237 reached. A higher conversion was also obtained when temperature was increased in
238 several studies dealing with pyrolysis-reforming of biomass [11,40-42], reforming of
239 the bio-oil aqueous fraction [43-45] and reforming of raw bio-oil [46-48].

240 Concerning the evolution of conversion with time on stream, at 550 ºC it decreases from
241 58.3 to 36.9 % in 20 min. However, between 600 and 700 ºC the decrease in conversion
242 with time on stream is not very significant until 70-80 min on stream, and subsequently
243 is very pronounced, with this trend being slightly less pronounced at 700 ºC. As
244 observed, there is an acceleration of deactivation with time on stream once the catalyst
245 starts deactivating and the concentration of non-reformed oxygenated compounds
246 increases in the reaction medium. This trend is attributable to the role of these
247 oxygenated compounds as coke precursors, which is well-established in the literature
248 for bio-oil reforming [25,49]. These authors highlight the fact that coke formation takes
249 place by decomposition of oxygenated compounds, eq. (10), and re-polymerization of
250 phenolic compounds derived from lignin pyrolysis:

251 $$C_nH_mO_k \rightarrow C_xH_yO_z + pyrolytic\ lignin\ (coke) \quad (11)$$

252 Remiro et al. [27] attenuate the impact of this coke formation mechanism in the
253 reforming of bio-oil by a controlled deposition of pyrolytic lignin, which reduces the
254 concentration of phenolic compounds fed into the reforming reactor.

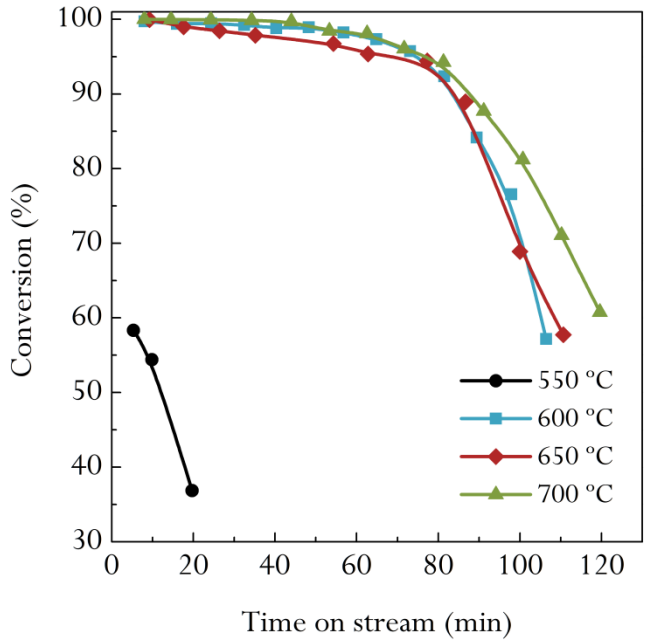


255

256 **Figure 2.** Effect of reforming temperature on the evolution of conversion with time on
257 stream. Reforming conditions: space time, 20 $g_{cat}$ min $g_{volatiles}^{-1}$; S/B ratio, 4.

258 Figure 3 shows the evolution of the yields of $H_2$, $CO_2$, CO, $CH_4$, $C_2$-$C_4$ hydrocarbons
259 (mainly ethylene, ethane, propylene and propane) and oxygenated compounds (non-
260 converted fraction) with time on stream, at 550 (a), 600 (b), 650 (c) and 700 ºC (d).
261 Initial $H_2$ yield increases from 54.4 % at 550 ºC to around 93.5 % in the 600-700 ºC
262 range, which corresponds to an increase in $H_2$ production from 6.4 to around 11.0 wt%.
263 Higher initial $H_2$ yields and productions are also obtained by several authors as
264 reforming temperature is increased in the pyrolysis and in-line reforming of biomass in
265 other reactors [11,37], which is due to the higher extent of the reforming reaction.
266 Similarly, studies dealing with bio-oil reforming confirm a similar trend for $H_2$ yield
267 [43,44,46-48,50].

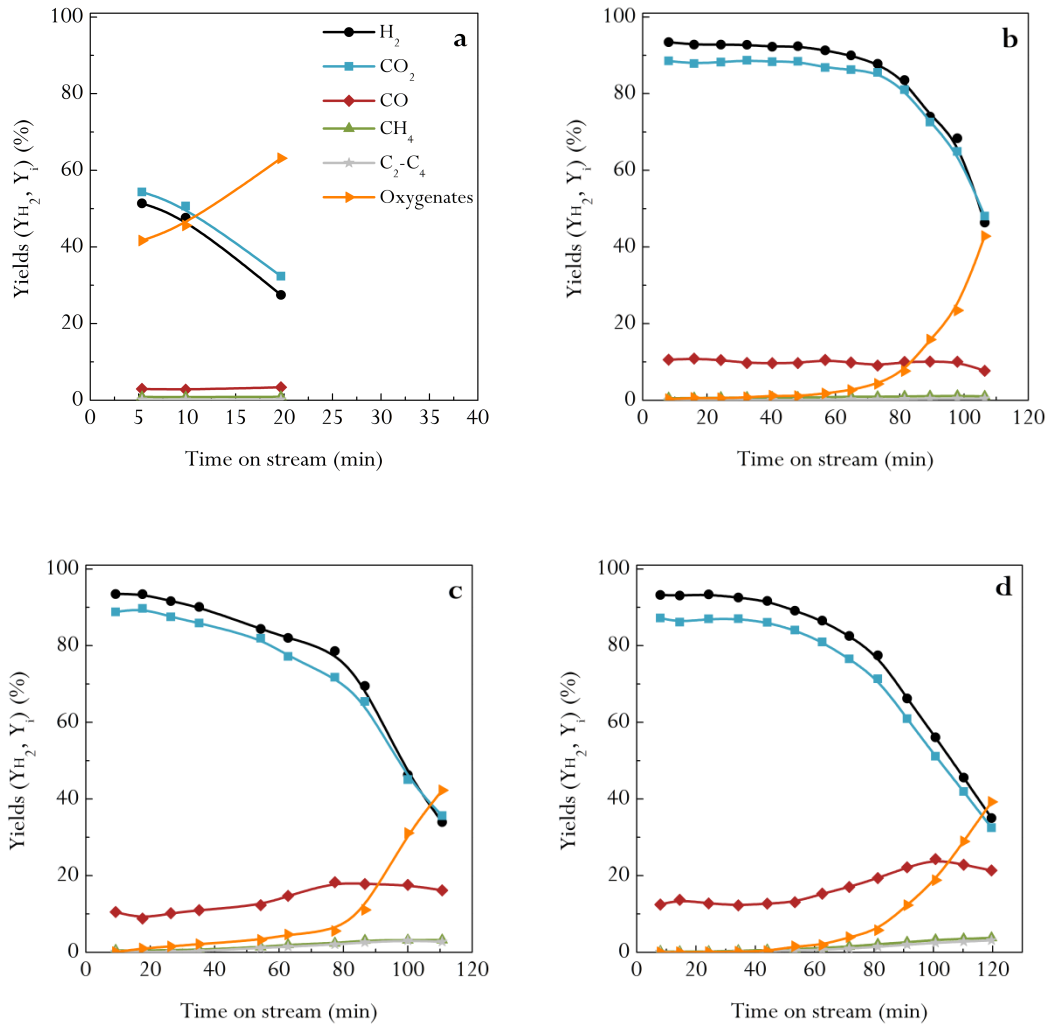


**Figure 3.** Effect of reforming temperature on the evolution of product yields with time on stream at 550 ºC (a), 600 ºC (b), 650 ºC (c) and 700 ºC (d). Reforming conditions: space time, 20 $g_{cat}$ min $g_{volatiles}^{-1}$; S/B ratio, 4.

Moreover, it should be pointed out that $H_2$ yield decreases with time on stream due to catalyst deactivation with the same trend shown in Figure 2 for conversion, with the initial decrease being more pronounced at 550 ºC (Figure 3a), from 51.4 at zero time on stream to 27.5 % in 20 min, due to the increase in oxygenate concentration in the reaction medium. At 600 ºC, and higher temperatures, the decrease in $H_2$ yield is only significant after a certain value of time on stream, which is caused by the autocatalytic effect of catalyst deactivation mentioned above due to the increase in the concentration of non-reformed oxygenates in the reaction medium. Accordingly, at 600 ºC $H_2$ yield decreases slowly from 93.5 at zero time on stream to 87.8 % in 75 min, with the

decrease being subsequently more pronounced down to 46.4 % in a period of 30 min approximately. $H_2$ yield follows a similar trend at 650 and 700 ºC, although the decrease is more pronounced than that observed at 600 ºC for the first 75 min, i.e., decreases from 93.5 to 78.6 % in 77 min at 650 ºC and from 93.2 to 82.5 % in 72 min at 700 ºC. Furthermore, $CO_2$ yield follows a similar trend as $H_2$ yield with time on stream, obtaining a similar value at all temperatures when the catalyst is deactivated. Regarding CO yield, it is maintained almost constant at 550 (~ 3 %) and 600 ºC (~ 10 %), whereas it increases slightly with time on stream from 10.5 to 16.2 % in 110 min at 650 ºC and from 12.5 to 21.4 % in 120 min at 700 ºC. This effect of temperature on CO yield is attributable to the higher oxygenate decomposition rate, eq. (10), and the displacement of the thermodynamic equilibrium of WGS reaction when temperature is increased. The increase in CO yield with time on stream is also a consequence of favouring the reaction of oxygenate decomposition (eq. (10)) due to the higher concentration of these compounds in the reaction medium, given that the catalyst is deactivated for reforming reactions. Catalyst deactivation for WGS reaction can also contribute to these results.

In the 600-700 ºC range (Figures 3b-d), and as a consequence of the decrease in catalyst activity for the reforming reactions, the yields of $CH_4$, $C_2$-$C_4$ hydrocarbons (overlapped results) and non-converted oxygenates increase with time on stream in the whole temperature range studied, with the increase being exponential as catalyst deactivation is more severe. This trend is explained by thermal cracking reactions of oxygenated compounds to form $CH_4$ and $C_2$-$C_4$ hydrocarbons, eq. (10), which occurs in parallel with the reforming reactions. Consequently, as the rate of the reforming reactions decreases due to catalyst deactivation, the formation of products by thermal cracking reactions is favoured.

In order to explain the effect temperature has on catalyst deactivation, the coke deposited at different temperatures has been analyzed by temperature programmed oxidation (TPO) and transmission electron microscopy (TEM) techniques. Thus, Figure 4 displays the TPO profiles of the deactivated catalyst (Figure 4a) and the amount of coke deposited (Figure 4b) at the reforming temperatures studied. Considering the different peaks observed in the TPO profile (Figure 4a), two different types of cokes may be distinguished, which are burnt at different temperatures. These different types of cokes have also been identified in deactivated Ni-based catalysts in the reforming of $CH_4$ [51,52], hydrocarbons [15,53-55] and oxygenated compounds, such as ethanol [56-

61]. In these works, the coke that burns a low temperatures (< 450 ºC) (coke I) is defined as amorphous coke and encapsulates Ni metallic sites (which promote its combustion), whereas the coke burning at higher temperatures (coke II) is separated from Ni active sites, more structured and evolves towards higher graphitization structures, even forming filamentous coke and carbon nanotubes (less common in the reforming of oxygenates and bio-oil).

As shown in Figure 4a, an increase in reforming temperature causes the displacement of the peaks corresponding to the different types of cokes towards higher combustion temperatures. In the case of the amorphous coke, there is a pronounced displacement of its combustion peak as reforming temperature is increased from 550 to 600 ºC, with the tops of the peaks being placed at around 380 and 425 ºC, respectively. In the case of the structured coke, the effect of reforming temperature on peak position is less significant, with the top being placed at around 550, 560, 610 and 620 ºC for the reforming temperatures of 550, 600, 650 and 700 ºC, respectively. This displacement is explained by the evolution of the coke to more condensed structures when reforming temperature is increased [62], making more difficult its combustion due to the less hydrogenated nature of the coke and its location in the catalyst particle farther from Ni sites.

Moreover, Figure 4b shows the effect temperature has on the amount of the different types of cokes. It should be pointed out that the amount of coke has been given per mass unit of biomass fed into the system, given that reaction time is different in each experiment, as they were stopped when the catalyst was deactivated. Consequently, the values in Figure 4b are the average rates of coke deposition. Table 2 shows the values of coke content ($C_C$), the reaction time, the biomass fed into the system and the amount of coke deposited per biomass mass unit ($C_C$').

As observed in Figure 4b, the amount of coke deposited per biomass mass unit on Ni active sites (coke I) decreases considerably when temperature is increased from 550 ºC to 600 ºC, with the decrease being less pronounced at higher temperatures. On the contrary, the amount of coke separated from Ni sites (coke II) increases steadily when temperature is increased, especially in the 600-650 ºC range. As a consequence of the different trend of the two types of cokes, the amount of coke per biomass mass unit has a minimum value at 600 ºC and increases from 1.25 to 2.37 $mg_{coke}\ g_{cat}^{-1}\ g_{biomass}^{-1}$ in the

600-700 ºC range. Wang et al. [63] also observed that the total amount of coke deposited on the catalyst was higher when temperature was increased.

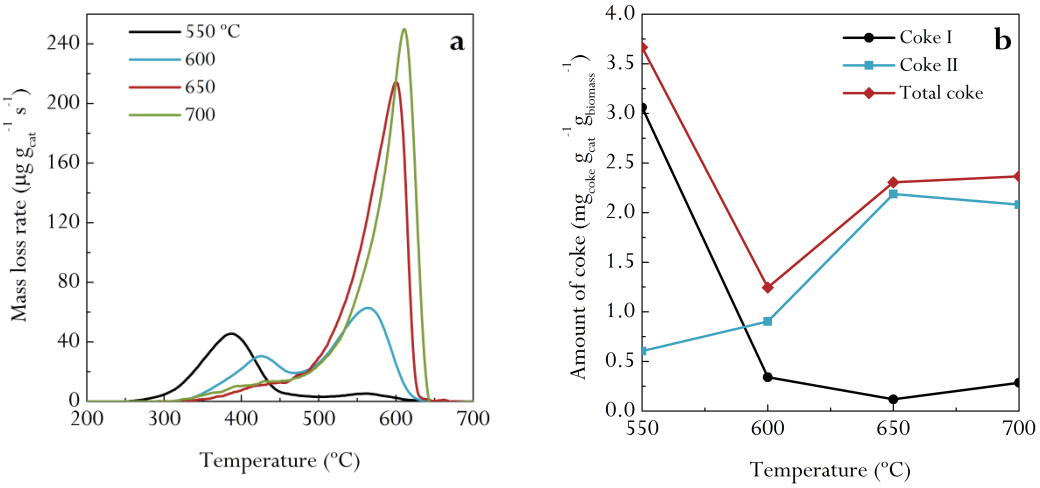


**Figure 4.** Effect of reforming temperature on the TPO profiles of the deactivated catalyst (a) and total amount of coke deposited per biomass mass unit (b). Reforming conditions: space time, 20 $g_{cat}$ min $g_{volatiles}^{-1}$; S/B ratio, 4.

**Table 2.** Total coke content in the catalyst ($C_C$) and the total amount of coke deposited per biomass mass unit ($C_C'$) at different reforming temperatures. Reforming conditions: space time, 20 $g_{cat}$ min $g_{volatiles}^{-1}$; S/B ratio, 4.

| Temperature (ºC) | $C_C$ ($mg_{coke}$ $g_{cat}^{-1}$) | Time on stream (min) | Biomass feed (g) | $C_C'$ ($mg_{coke}$ $g_{cat}^{-1}$ $g_{biomass}^{-1}$) |
|---|---|---|---|---|
| 550 | 5.5 | 20 | 15 | 3.67 |
| 600 | 9.9 | 106 | 80 | 1.25 |
| 650 | 19.2 | 111 | 83 | 2.31 |
| 700 | 21.3 | 120 | 90 | 2.37 |

Comparing the results in Figure 4b with those corresponding to the evolution with time on stream in Figures 2 and 3, catalyst deactivation is not directly related to coke content, but coke nature and location influences this deactivation, which in turn is related to the reaction conditions, with temperature and oxygenate concentration being of high significant. Thus, amorphous coke deposition is very high at 550 ºC due to the significance of oxygenate decomposition and polymerization reactions, eqs. (10) and (11), respectively, given that oxygenate concentration in the reaction medium is high at

363 this temperature. It is well-established in the literature [45,55,64,65] that amorphous
364 coke is the main responsible for catalyst deactivation because it encapsulates Ni sites.
365 Above 600 ºC, oxygenate reforming reactions are favoured rather than thermal
366 reactions, and presumably the gasification of the amorphous coke is also enhanced
367 because it is located close to Ni particles. Moreover, oxygenate concentration in the
368 reaction medium is lower when temperature is increased, and therefore their
369 decomposition and polymerization reaction rates undergo attenuation. On the contrary,
370 the amount of coke II (which is burnt at higher temperatures) deposited on the catalyst
371 per biomass mass unit increases when reforming temperature is increased (Figure 4b),
372 attaining its maximum content at 700 ºC. This trend at high temperatures is explained
373 by the evolution of amorphous coke towards more refractory structures with lower
374 capacity for Ni site blockage and gasification [61,62]. The high temperature needed for
375 its combustion by TPO in Figure 4a (620 ºC for a reforming temperature of 700 ºC)
376 reveals the graphitic nature of coke II at this temperature. Moreover, the effect
377 temperature has on the content of each type of coke cannot be clearly ascertained due to
378 the different duration of the reactions. Thus, the duration of the reaction at 550 ºC is
379 short, and therefore the coke does not evolve towards more condensed structures.
380 Furthermore, the contribution of Boudouard (eq. (12)) and $CH_4$ decomposition (eq.
381 (13)) reactions to the formation of coke II cannot be excluded at high temperatures.

382 $$2CO \leftrightarrow CO_2 + C(coke) \quad (12)$$

383 $$CH_4 \rightarrow 2H_2 + C(coke) \quad (13)$$

384 Figure 5 shows the images of transmission electron microscopy (TEM) of the catalyst
385 deactivated at 600 ºC (Figure 5a) and 700 ºC (Figure 5b), in which Ni particles are
386 identified as dark areas. As observed, all Ni particles are coated with coke, whose
387 structure is more ordered when temperature is increased.

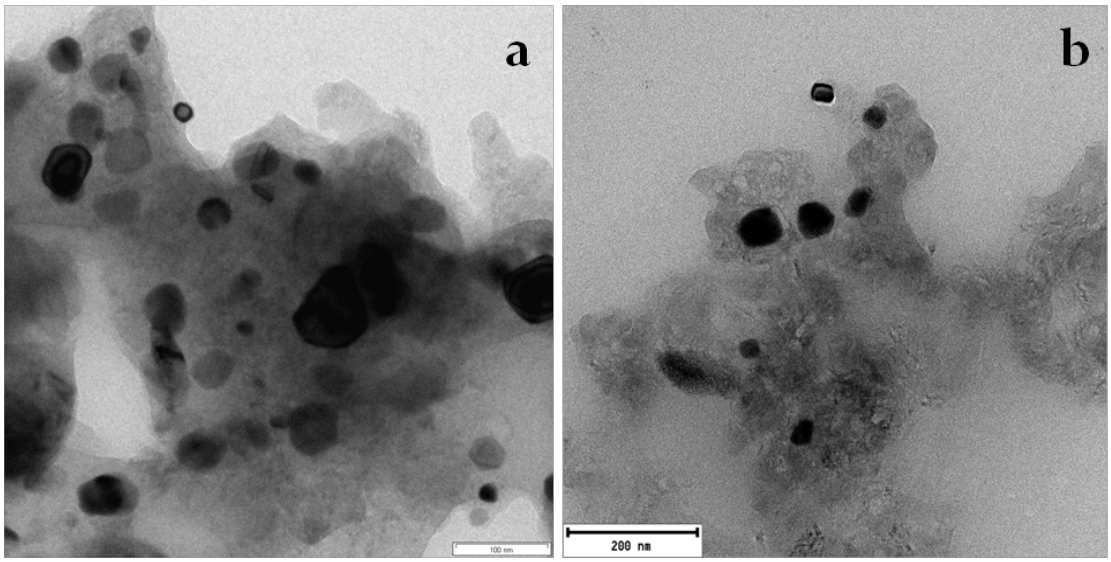


**Figure 5.** TEM images of the catalyst deactivated at 600 ºC (a) and 700 ºC (b). Operating conditions: space time, 20 $g_{cat}$ min $g_{volatiles}^{-1}$; S/B ratio, 4.

Filamentous coke is not observed in Figure 5, which is because the coke has a more disordered structure than in the reforming of other oxygenated compounds, such as ethanol [56,57,60] and, particularly, in the reforming of hydrocarbons [15,53,54]. Concerning biomass valorisation, the research group headed by Prof. Williams studied Ni-based deactivated catalysts in the pyrolysis and in-line reforming of biomass in batch regime, verifying that the composition of biomass pyrolysis products (with high content of phenols and water) is not suitable for the production of nano-structured materials and coke nature depends on the catalyst. Accordingly, Efika et al. [22] verified by SEM images the presence of filamentous carbon in a $Ni/Al_2O_3$ catalyst, whereas carbon filaments are not clearly observed in a $Ni/CeO_2/Al_2O_3$ catalyst. Nahil et al. [23] observed two different carbon oxidation peaks in their TPO curve, one at around 450 ºC (amorphous coke) and the other one at around 550 ºC (filamentous coke). However, when rice husk, sugar cane bagasse and wheat straw were used as feedstock, the second peak was obtained at around 650 ºC, which was assigned to graphitic carbon [24].

### 3.2. Effect of reforming space time

According to the results aforementioned in Section 3.1, 600 ºC is the suitable temperature for attenuating catalyst deactivation and higher temperatures are not interesting due to the higher energy costs involved. Accordingly, the effect space time has on deactivation has been studied based on runs at 600 ºC with a S/B ratio of 4 and

space times of 10, 15, 20 and 30 $g_{cat}$ min $g_{volatiles}^{-1}$. Figure 6 shows the effect space time has on the evolution of conversion of pyrolysis volatiles with time on stream. As observed, when space time is increased a higher initial conversion is obtained, which has also been reported in several biomass pyrolysis-reforming studies [66,67]. Thus, an initial conversion higher than 98.5 % is obtained above 15 $g_{cat}$ min $g_{volatiles}^{-1}$, with the maximum conversion (and tar-free gas) being obtained with 20 $g_{cat}$ min $g_{volatiles}^{-1}$.

Concerning the evolution of conversion with time on stream (Figure 6), catalyst deactivation is attenuated when space time is increased, which is explained by the role played by the non-converted oxygenated compounds as coke precursors. A higher lifespan of the catalyst at high space times is obtained in the reforming of bio-oil [27,68]. Therefore, almost full conversion is achieved in the first 160 min when a space time of 30 $g_{cat}$ min $g_{volatiles}^{-1}$ is used, whereas catalyst deactivation is significant for times on stream longer than 60 min when using 20 $g_{cat}$ min $g_{volatiles}^{-1}$, with the decrease in activity being pronounced subsequent to 75 min. Furthermore, when a space time lower than 15 $g_{cat}$ min $g_{volatiles}^{-1}$ is used, the decrease in conversion is significant after 20 min on stream.

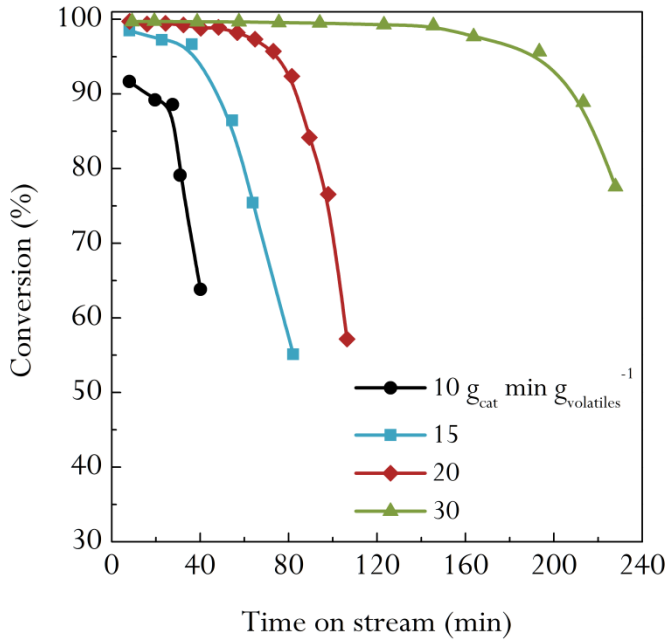


**Figure 6.** Effect of reforming space time on the evolution of conversion with time on stream. Reforming conditions: 600 ºC; S/B ratio, 4.

Figure 7 shows the effect space time has on the evolution of product yields with time on stream. When space time is increased, higher $H_2$ yields are obtained at zero time on stream due to the higher extent of reforming and WGS reactions, which is consistent with the literature on the reforming of bio-oil [6,48,69,70]. Moreover, the effect space time has on the initial CO and $CO_2$ yields is noteworthy. As observed, when space time is increased from 10 to 20 $g_{cat}$ min $g_{volatiles}^{-1}$ (Figures 7a and 7c, respectively) the initial CO yield increases from 7.9 to 10.6 % and the initial $CO_2$ yield from 82.1 to 88.6 %. However, the initial CO yield decreases to 6.7 % and that of $CO_2$ increases to 92.6 % at the highest space time studied (Figure 7d), with the yields of $CH_4$ and $C_2$-$C_4$ hydrocarbons being lower. This trend for CO and $CO_2$ yields when space time is increased is also reported in the literature for bio-oil reforming [9,43,71] and is evidence that both reforming and WGS reactions are favoured at low space time values, whereas the WGS reaction is more favoured than reforming reactions at high space time values.

Concerning the evolution with time on stream of the product yields shown in Figure 7, the decrease in $H_2$ yield is lower at high space time values, i.e., from 84.9 to 55.0 % in 40 min with 10 $g_{cat}$ min $g_{volatiles}^{-1}$ and from 95.8 to 63.3 % in 230 min with 30 $g_{cat}$ min $g_{volatiles}^{-1}$. Furthermore, the effect space time has on the decrease of $CO_2$ yield follows a similar trend, whereas CO yield does not follow a clear trend, with its value being between 6 and 10 %. The slight effect of space time is evidence that the decrease expected in the reforming rate due to catalyst deactivation is compensated with the higher formation of CO by cracking of oxygenates, whose concentration is higher as the catalyst is being deactivated. In addition, the presence of CO is also favoured by catalyst deactivation for WGS reaction. However, the decrease in the rate of reforming reactions is also evident, i.e., the yields of $CH_4$ and $C_2$-$C_4$ hydrocarbons increase exponentially when time on stream increases (overlapped results), which is explained by the increase in the yield of non-converted oxygenates in the reaction environment. Therefore, cracking reactions are favoured, enhancing the formation of $CH_4$ and $C_2$-$C_4$ hydrocarbons [27,44,71,72].

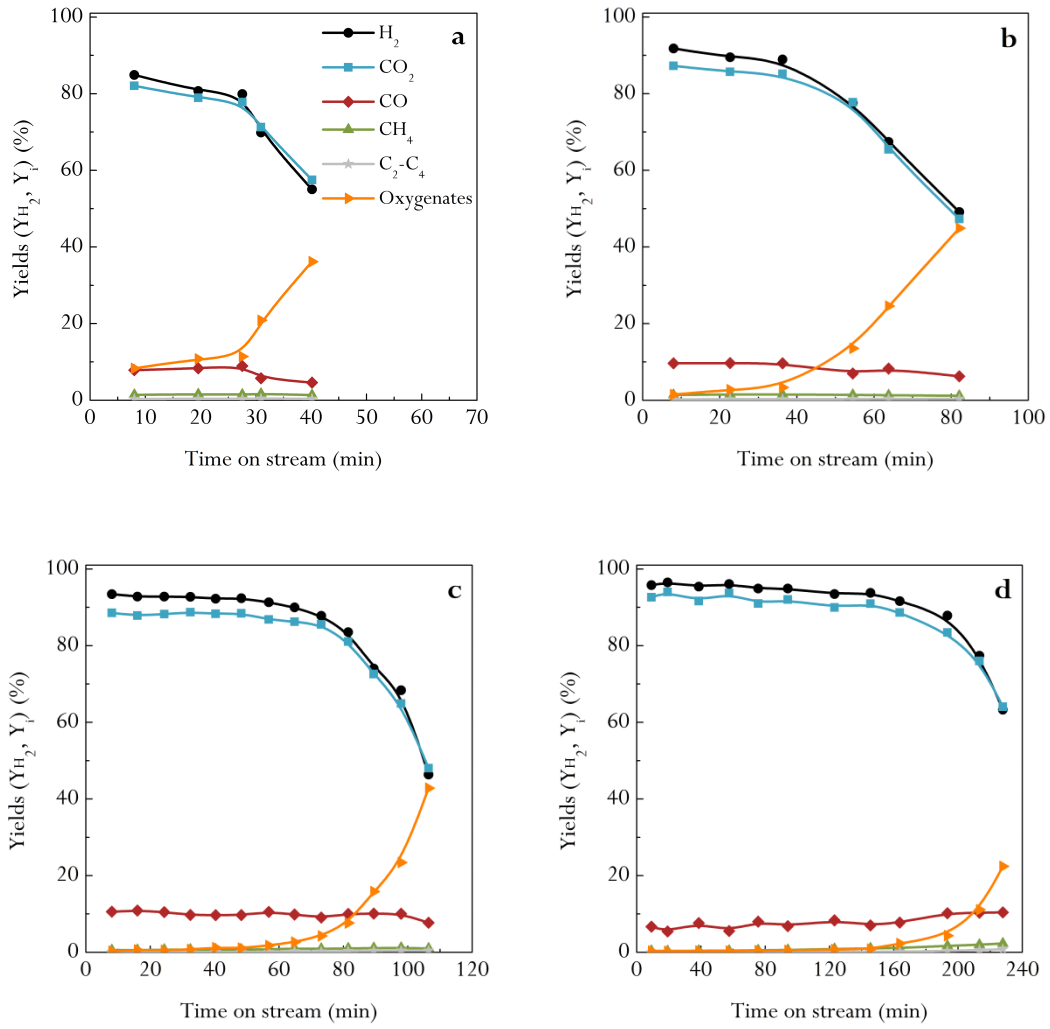


**Figure 7.** Effect of reforming space time on the evolution of product yields with time on stream when using 10 (a), 15 (b), 20 (c) and 30 $g_{cat}$ min $g_{volatiles}^{-1}$ (d). Reforming conditions: 600 ºC; S/B ratio, 4.

Figure 8a displays the TPO results obtained in the experiments carried out using different space times. Moreover, Figure 8b and Table 3 show the coke contents of the deactivated catalyst. As aforementioned, the fact of using different catalyst masses and times on stream in each experiment (Table 3) has to be considered when comparing the results in Figure 8b, in which the coke contents deposited per biomass mass unit fed into the system are shown. As observed, the total amount of coke per biomass mass unit decreases from 1.83 to 0.29 $mg_{coke}$ $g_{cat}^{-1}$ $g_{biomass}^{-1}$ when space time is increased in the 10-30 $g_{cat}$ min $g_{volatiles}^{-1}$ range, given that a higher amount of catalyst enhances reforming reactions and reduces oxygenate concentration, which are the main coke precursors.

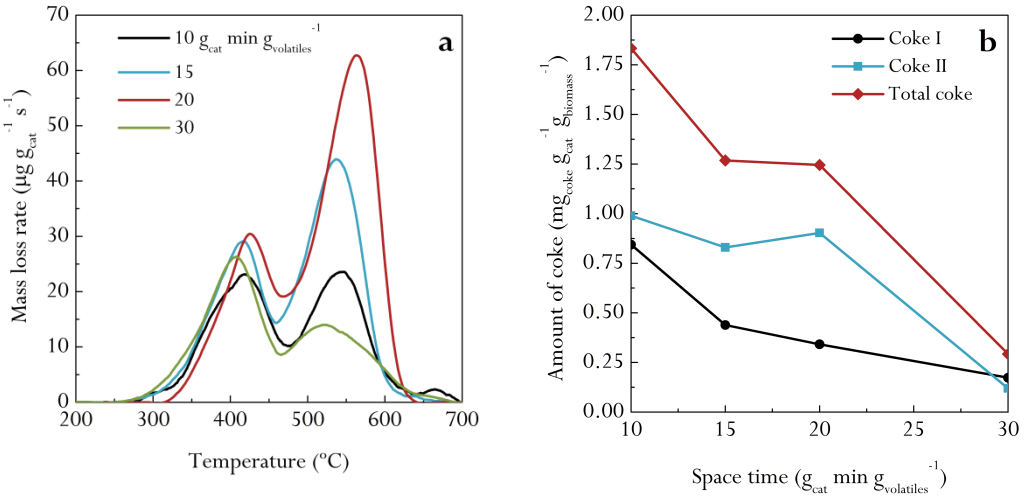


471

472 **Figure 8.** Effect of space time on the TPO profiles of the deactivated catalyst (a) and
473 total amount of coke deposited per biomass mass unit (b). Reforming conditions: 600
474 ºC; S/B ratio, 4.

475 **Table 3.** Total coke content in the catalyst ($C_C$) and the total amount of coke deposited
476 per biomass mass unit ($C_C'$) at different space times. Reforming conditions: 600 ºC; S/B
477 ratio, 4.

| Space time ($g_{cat}$ min $g_{volatiles}^{-1}$) | $C_C$ ($mg_{coke}$ $g_{cat}^{-1}$) | Time on stream (min) | Biomass feed (g) | $C_C'$ ($mg_{coke}$ $g_{cat}^{-1}$ $g_{biomass}^{-1}$) |
|---|---|---|---|---|
| 10 | 5.5 | 40 | 30 | 1.83 |
| 15 | 7.8 | 82 | 62 | 1.27 |
| 20 | 9.9 | 106 | 80 | 1.25 |
| 30 | 5.0 | 228 | 171 | 0.29 |

478

479 Considering the effect space time has on the amount of each type of coke deposited on
480 the catalyst, it can be observed in Figure 8b that the amount of coke I (which is burnt at
481 low temperatures) per biomass mass unit decreases from 0.84 to 0.17 $mg_{coke}$ $g_{cat}^{-1}$
482 $g_{biomass}^{-1}$ as space time is increased in the 10-30 $g_{cat}$ min $g_{volatiles}^{-1}$ range. This result can
483 be explained by the thermal origin of this coke, which is produced by decomposition of
484 oxygenates (eq. (10)) and re-polymerization of phenolic compounds on the catalyst
485 surface (eq. (11)). Consequently, the progress of these reactions is disfavoured by the
486 higher extent of oxygenate reforming and WGS reactions, as observed in the reforming
487 of bio-oil [6,25,27]. Similarly, when space time increases the amount of coke II
488 deposited per biomass mass unit decreases, given that presumably this coke is formed

mainly by evolution of the coke towards more ordered structures, and is separated from Ni active sites. Moreover, a displacement of this coke peak is observed when space time is increased in Figure 8a. This effect is a consequence of the higher duration of the reactions, and therefore a subsequent evolution of the coke to a more condensed structure. Nevertheless, this effect avoids the formation of coke II, which decreases when a space time of 30 $g_{cat}$ min $g_{volatiles}^{-1}$ is used, due to the lower concentration of oxygenated compounds in the reaction environment. These conditions, in which a high space time value is used, are interesting from an industrial point of view, as the deposition of coke is limited. Thus, when a space time of 30 $g_{cat}$ min $g_{volatiles}^{-1}$ is used, a maximum $H_2$ production of 11.7 wt % is obtained, with the catalyst being stable for more than 2 h.

### 3.3. Effect of S/B ratio

Figure 9 shows the evolution of conversion with time on stream using different S/B ratios. The results correspond to S/B ratios of 2, 3, 4 and 5 (S/C ratios of 3.9, 5.8, 7.7 and 9.7, respectively), at 600 ºC and a space time of 20 $g_{cat}$ min $g_{volatiles}^{-1}$. As observed, the conversion at zero time on stream increases slightly from 99.5 to 100 % when a high space time value is used and S/B ratio is increased from 2 to 5. However, the deactivation is attenuated considerably, in particular when S/B ratio is increased from 2 to 3. These results are explained by the lower concentration of oxygenated compounds (which are coke precursors) and the higher reforming rate of these oxygenates and intermediate compounds. However, above a S/B ratio of 4, its influence on conversion decrease is lower, which is attributable to the partial saturation of Ni active sites with adsorbed steam [73].

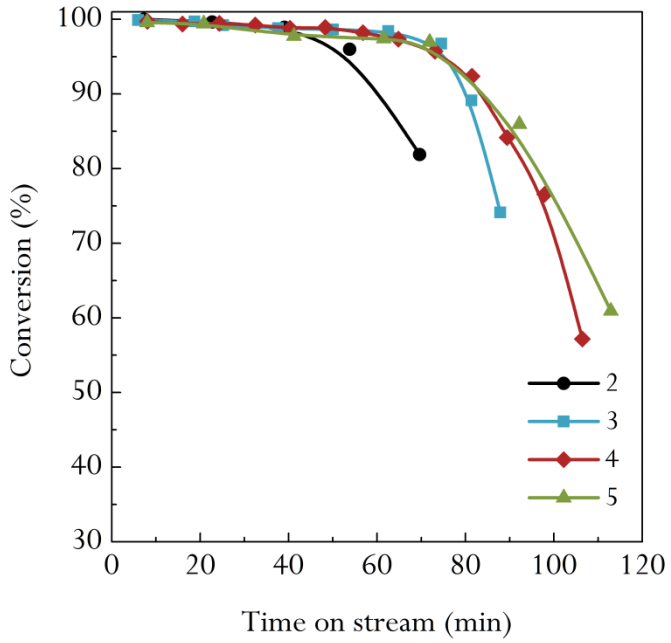


512

513 **Figure 9.** Effect of S/B ratio on the evolution of conversion with time on stream.
514 Reforming conditions: 600 ºC; space time, 20 $g_{cat}$ min $g_{volatiles}^{-1}$.

515 Figure 10 shows the effect of S/B ratio on the evolution of product yields with time on
516 stream. Most authors reported that a higher initial $H_2$ yield is obtained when S/B ratio is
517 increased in the reforming of bio-oil [47,48,65,74]. In this study, the initial $H_2$ yield
518 increases from 89.2 to 94.2 % when S/B ratio is increased in the 2-5 range, due to the
519 enhancement of reforming and WGS reactions, with $CO_2$ yield being higher and CO
520 yield lower.

521 As mentioned above for conversion, the effect on catalyst deactivation is not so
522 significant at high S/B ratios. Moreover, it should be noted that the yields of $CH_4$ and
523 $C_2$-$C_4$ hydrocarbons (produced by oxygenate decomposition reactions) and the presence
524 of oxygenated compounds in the reaction environment is delayed when high S/B ratios
525 are used, which has also been reported in studies dealing with the reforming of bio-oil
526 [6,50,69,74]. The aforementioned results reveal the interest of using an S/B ratio of 3,
527 with $H_2$ yield being constant (around 93 %) for 70 min under the conditions studied. A
528 higher S/B ratio only improves slightly the deactivation results and has as counterpart
529 higher energy requirements for water vaporization.

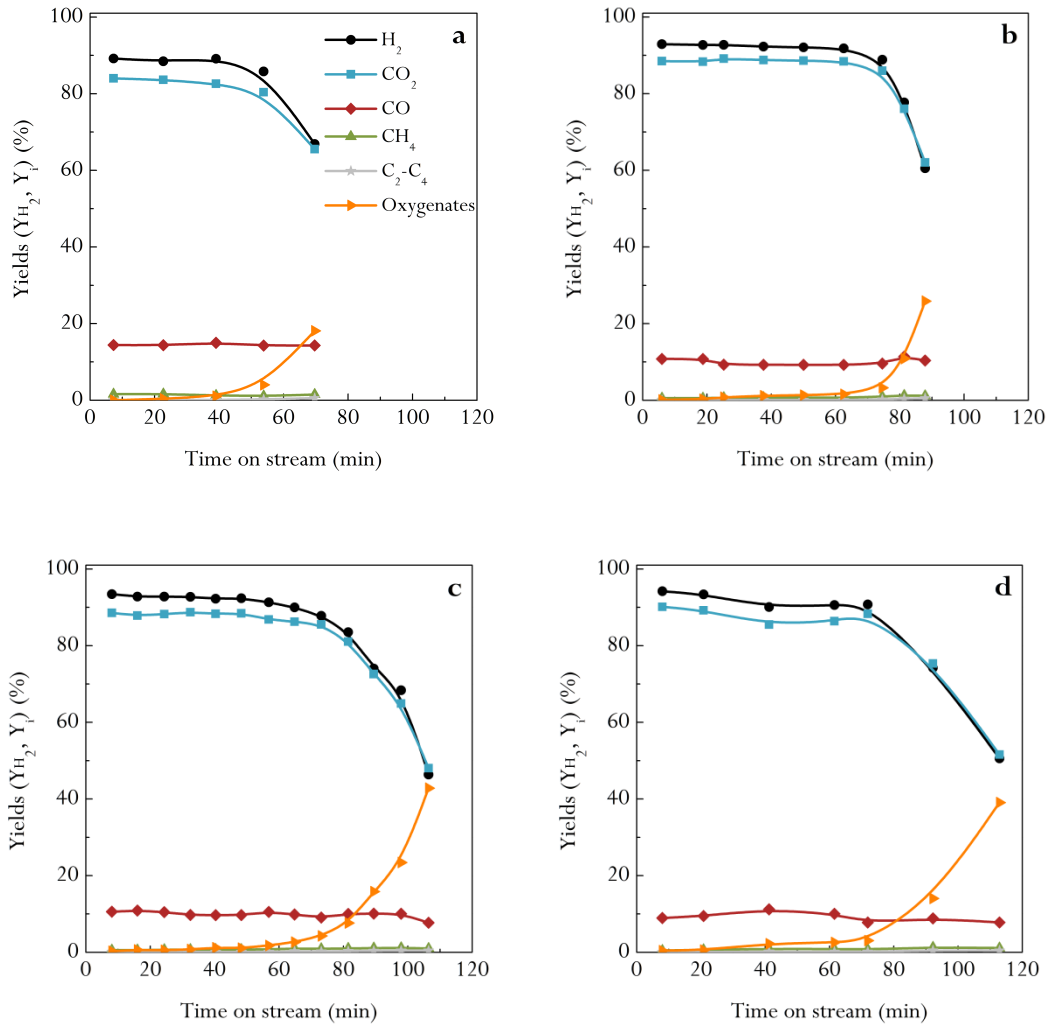


**Figure 10.** Effect of S/B ratio on the evolution of product yields with time on stream with S/B ratios of 2 (a), 3 (b), 4 (c) and 5 (d). Reforming conditions: 600 ºC; space time, 20 $g_{cat}$ min $g_{volatiles}^{-1}$.

Figure 11a displays the TPO profiles for the catalyst deactivated at different S/B ratios and Figure 11b and Table 4 show the effect S/B ratio has on the amount of each type of coke deposited on the catalyst. Thus, the amount of coke deposited per biomass mass unit decreases from 1.38 to 0.83 $mg_{coke}$ $g_{cat}^{-1}$ $g_{biomass}^{-1}$ when S/B ratio is increased from 2 to 5, which has also been verified in the reforming of bio-oil [48,63,68]. Nevertheless, the effect S/B ratio has on the formation of each type of coke is different. The amount of coke I is almost constant when S/B ratio is increased, which is evidence that the formation of amorphous coke (through the reactions in eqs. (10) and (11)) only depends on temperature. However, the formation of coke II is disfavoured when S/B ratio is increased, given that the condensation of coke I components is attenuated. The fact that

catalyst deactivation is lower when S/B ratio is increased (Figures 9 and 10), with the amount of coke I being similar, is evidence that an increase in steam concentration is not effective for attenuating amorphous coke deposition, but avoids the isolation of Ni active sites, and therefore the effective deactivation is attenuated.

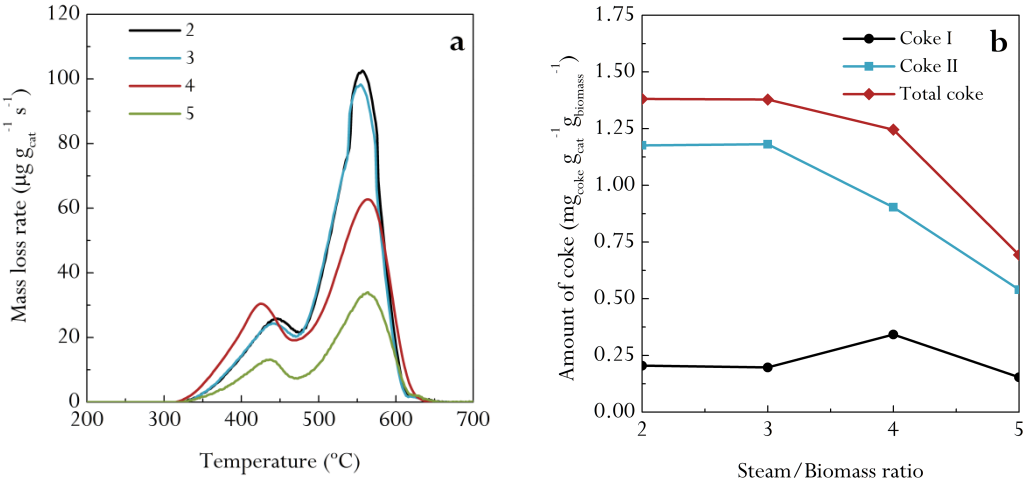


**Figure 11.** Effect of steam/biomass ratio on the TPO profiles of the deactivated catalyst (a) and total amount of coke deposited per biomass mass unit (b). Reforming conditions: temperature, 600 ºC, space time, 20 $g_{cat}$ min $g_{volatiles}^{-1}$.

**Table 4.** Total coke content in the catalyst ($C_C$) and total amount of coke deposited per biomass mass unit ($C_C'$) at different S/B ratios. Reforming conditions: 600 ºC; space time, 20 $g_{cat}$ min $g_{volatiles}^{-1}$.

| S/B ratio | $C_C$ ($mg_{coke}$ $g_{cat}^{-1}$) | Time on stream (min) | Biomass feed (g) | $C_C'$ ($mg_{coke}$ $g_{cat}^{-1}$ $g_{biomass}^{-1}$) |
|---|---|---|---|---|
| 2 | 14.5 | 70 | 105 | 1.38 |
| 3 | 11.3 | 82 | 82 | 1.38 |
| 4 | 9.9 | 106 | 80 | 1.25 |
| 5 | 4.7 | 113 | 68 | 0.69 |

## Conclusions

The good performance of a two in-line reactor system (CSBR-FBR) for biomass pyrolysis-reforming has been proven in a wide range of operating conditions. Nevertheless, the catalyst undergoes a severe deactivation with time on stream related to coke deposition, whose formation is attributable to the decomposition of oxygenated

compounds and the re-polymerization of phenolic oxygenates. The TPO analysis of the coke allows identifying two different fractions, corresponding to the coke deposited on Ni active sites and the coke separated from these sites. Coke deposition and the resulting deactivation can be attenuated by selecting operating conditions in which the reforming and WGS reactions are favoured, and therefore the concentration of oxygenates (coke precursors) in the reaction medium is minimized. In order to achieve these objectives, a temperature of 600 ºC and a S/B ratio of 3 have been chosen as suitable conditions. Moreover, catalyst stability is favoured when space time is increased, and a $H_2$ yield of 95.8 % is achieved for 160 min on stream for a space time of 30 $g_{cat}$ min $g_{volatiles}^{-1}$.

Catalyst deactivation is a problem for the scaling up of the process. However, the fluidized bed reactor is suitable to carry out the reforming step with catalyst circulation, with the catalyst being regenerated by coke combustion in another unit. In this case, the regenerated catalyst would partially contribute to providing the energy required in the reforming step.

## Acknowledgement

This work was carried out with financial support from the Ministry of Economy and Competitiveness of the Spanish Government (CTQ2016-75535-R (AEI/FEDER, UE) and CTQ-2015-69436-R (AEI/FEDER, UE)), the Basque Government (IT748-13) and the University of the Basque Country (UFI 11/39). I. Barbarias thanks the University of the Basque Country for her postgraduate grant (UPV/EHU 2016).

## References

[1] Ayalur Chattanathan S, Adhikari S, Abdoulmoumine N. A review on current status of hydrogen production from bio-oil. Renewable Sustainable Energy Rev 2012;16:2366-72.

[2] Gollakota ARK, Reddy M, Subramanyam MD, Kishore N. A review on the upgradation techniques of pyrolysis oil. Renewable Sustainable Energy Rev 2016;58:1543-68.

[3] Guan G, Kaewpanha M, Hao X, Abudula A. Catalytic steam reforming of biomass tar: Prospects and challenges. Renewable Sustainable Energy Rev 2016;58:450-61.

[4] Bridgwater AV. Review of fast pyrolysis of biomass and product upgrading. Biomass Bioenergy 2012;38:68-94.

[5] Kan T, Strezov V, Evans TJ. Lignocellulosic biomass pyrolysis: A review of product properties and effects of pyrolysis parameters. Renewable Sustainable Energy Rev 2016;57:126-1140.

[6] Remiro A, Valle B, Aguayo AT, Bilbao J, Gayubo AG. Steam reforming of raw bio-oil in a fluidized bed reactor with prior separation of pyrolytic lignin. Energy Fuels 2013;27:7549-59.

[7] Seyedeyn-Azad F, Abedi J, Sampouri S. Catalytic steam reforming of aqueous phase of bio-oil over Ni-based alumina-supported catalysts. Ind Eng Chem Res 2014;53:17937-44.

[8] Remón J, Broust F, Volle G, García L, Arauzo J. Hydrogen production from pine and poplar bio-oils by catalytic steam reforming. Influence of the bio-oil composition on the process. Int J Hydrogen Energy 2015;40:5593-608.

[9] Basagiannis AC, Verykios XE. Steam reforming of the aqueous fraction of bio-oil over structured $Ru/MgO/Al_2O_3$ catalysts. Catal Today 2007;127:256-64.

[10] Kechagiopoulos PN, Voutetakis SS, Lemonidou AA, Vasalos IA. Hydrogen production via reforming of the aqueous phase of bio-oil over Ni/olivine catalysts in a spouted bed reactor. Ind Eng Chem Res 2009;48:1400-8.

[11] Xiao X, Cao J, Meng X, et al. Synthesis gas production from catalytic gasification of waste biomass using nickel-loaded brown coal char. Fuel 2013;103:135-40.

[12] Chen F, Wu C, Dong L, Vassallo A, Williams PT, Huang J. Characteristics and catalytic properties of $Ni/CaAlO_x$ catalyst for hydrogen-enriched syngas production from pyrolysis-steam reforming of biomass sawdust. Appl Catal B 2016;183:168-75.

[13] Arregi A, Lopez G, Amutio M, Barbarias I, Bilbao J, Olazar M. Hydrogen production from biomass by continuous fast pyrolysis and in-line steam reforming. RSC Adv 2016;6:25975-85.

[14] Dong L, Wu C, Ling H, Shi J, Williams PT, Huang J. Promoting hydrogen production and minimizing catalyst deactivation from the pyrolysis-catalytic steam reforming of biomass on nanosized $NiZnAlO_x$ catalysts. Fuel 2017;188:610-20.

[15] Barbarias I, Lopez G, Alvarez J, et al. A sequential process for hydrogen production based on continuous HDPE fast pyrolysis and in-line steam reforming. Chem Eng J 2016;296:191-8.

[16] Barbarias I, Lopez G, Artetxe M, et al. Pyrolysis and in-line catalytic steam reforming of polystyrene through a two-step reaction system. J Anal Appl Pyrolysis 2016;122:502-10.

[17] Arregi A, Amutio M, Lopez G, et al. Hydrogen-rich gas production by continuous pyrolysis and in-line catalytic reforming of pine wood waste and HDPE mixtures. Energy Convers Manage 2017;136:192-201.

631 [18] Erkiaga A, Lopez G, Amutio M, Bilbao J, Olazar M. Influence of operating
632 conditions on the steam gasification of biomass in a conical spouted bed reactor. Chem
633 Eng J 2014;237:259-67.

634 [19] Alvarez J, Lopez G, Amutio M, Bilbao J, Olazar M. Upgrading the rice husk char
635 obtained by flash pyrolysis for the production of amorphous silica and high quality
636 activated carbon. Bioresour Technol 2014;170:132-7.

637 [20] Amutio M, Lopez G, Alvarez J, Olazar M, Bilbao J. Fast pyrolysis of eucalyptus
638 waste in a conical spouted bed reactor. Bioresour Technol 2015;194:225-32.

639 [21] Erkiaga A, Lopez G, Barbarias I, et al. HDPE pyrolysis-steam reforming in a
640 tandem spouted bed-fixed bed reactor for $H_2$ production. J Anal Appl Pyrolysis
641 2015;116:34-41.

642 [22] Efika CE, Wu C, Williams PT. Syngas production from pyrolysis-catalytic steam
643 reforming of waste biomass in a continuous screw kiln reactor. J Anal Appl Pyrolysis
644 2012;95:87-94.

645 [23] Nahil MA, Wang X, Wu C, Yang H, Chen H, Williams PT. Novel bi-functional
646 Ni-Mg-Al-CaO catalyst for catalytic gasification of biomass for hydrogen production
647 with in situ $CO_2$ adsorption. RSC Adv 2013;3:5583-90.

648 [24] Waheed QMK, Williams PT. Hydrogen production from high temperature
649 pyrolysis/steam reforming of waste biomass: Rice husk, sugar cane bagasse, and wheat
650 straw. Energy Fuels 2013;27:6695-704.

651 [25] Chen J, Sun J, Wang Y. Catalysts for Steam Reforming of Bio-oil: A Review. Ind
652 Eng Chem Res 2017;56:4627-37.

653 [26] Bartholomew CH. Mechanisms of catalyst deactivation. Appl Catal A
654 2001;212:17-60.

655 [27] Remiro A, Valle B, Aguayo AT, Bilbao J, Gayubo AG. Operating conditions for
656 attenuating Ni/$La_2O_3$- $\alpha Al_2O_3$ catalyst deactivation in the steam reforming of bio-oil
657 aqueous fraction. Fuel Process Technol 2013;115:222-32.

658 [28] Lopez G, Erkiaga A, Artetxe M, Amutio M, Bilbao J, Olazar M. Hydrogen
659 Production by High Density Polyethylene Steam Gasification and In-Line Volatile
660 Reforming. Ind Eng Chem Res 2015;54:9536-44.

661 [29] Alvarez J, Lopez G, Amutio M, Bilbao J, Olazar M. Bio-oil production from rice
662 husk fast pyrolysis in a conical spouted bed reactor. Fuel 2014;128:162-9.

663 [30] Elordi G, Olazar M, Lopez G, Artetxe M, Bilbao J. Continuous polyolefin cracking
664 on an HZSM-5 zeolite catalyst in a conical spouted bed reactor. Ind Eng Chem Res
665 2011;50:6061-70.

[31] Artetxe M, Lopez G, Amutio M, Elordi G, Bilbao J, Olazar M. Cracking of high density polyethylene pyrolysis waxes on HZSM-5 catalysts of different acidity. Ind Eng Chem Res 2013;52:10637-45.

[32] Erkiaga A, Lopez G, Amutio M, Bilbao J, Olazar M. Syngas from steam gasification of polyethylene in a conical spouted bed reactor. Fuel 2013;109:461-9.

[33] López G, Olazar M, Aguado R, Bilbao J. Continuous pyrolysis of waste tyres in a conical spouted bed reactor. Fuel 2010;89:1946-52.

[34] Lopez G, Olazar M, Aguado R, et al. Vacuum pyrolysis of waste tires by continuously feeding into a conical spouted bed reactor. Ind Eng Chem Res 2010;49:8990-7.

[35] Amutio M, Lopez G, Artetxe M, Elordi G, Olazar M, Bilbao J. Influence of temperature on biomass pyrolysis in a conical spouted bed reactor. Resour Conserv Recycl 2012;59:23-31.

[36] Li D, Ishikawa C, Koike M, Wang L, Nakagawa Y, Tomishige K. Production of renewable hydrogen by steam reforming of tar from biomass pyrolysis over supported Co catalysts. Int J Hydrogen Energy 2013;38:3572-81.

[37] Ma Z, Zhang S, Xie D, Yan Y. A novel integrated process for hydrogen production from biomass. Int J Hydrogen Energy 2014;39:1274-9.

[38] Chen F, Wu C, Dong L, Jin F, Williams PT, Huang J. Catalytic steam reforming of volatiles released via pyrolysis of wood sawdust for hydrogen-rich gas production on Fe-Zn/$Al_2O_3$ nanocatalysts. Fuel 2015;158:999-1005.

[39] Zou J, Yang H, Zeng Z, Wu C, Williams PT, Chen H. Hydrogen production from pyrolysis catalytic reforming of cellulose in the presence of K alkali metal. Int J Hydrogen Energy 2016;41:10598-607.

[40] Xiao X, Meng X, Le DD, Takarada T. Two-stage steam gasification of waste biomass in fluidized bed at low temperature: Parametric investigations and performance optimization. Bioresour Technol 2011;102:1975-81.

[41] Wang Y, Hu X, Song Y, et al. Catalytic steam reforming of cellulose-derived compounds using a char-supported iron catalyst. Fuel Process Technol 2013;116:234-40.

[42] Li D, Koike M, Chen J, Nakagawa Y, Tomishige K. Preparation of Ni-Cu/Mg/Al catalysts from hydrotalcite-like compounds for hydrogen production by steam reforming of biomass tar. Int J Hydrogen Energy 2014;39:10959-70.

[43] Bimbela F, Oliva M, Ruiz J, García L, Arauzo J. Hydrogen production via catalytic steam reforming of the aqueous fraction of bio-oil using nickel-based coprecipitated catalysts. Int J Hydrogen Energy 2013;38:14476-87.

[44] Liu S, Chen M, Chu L, et al. Catalytic steam reforming of bio-oil aqueous fraction for hydrogen production over Ni-Mo supported on modified sepiolite catalysts. Int J Hydrogen Energy 2013;38:3948-55.

[45] Yao D, Wu C, Yang H, et al. Hydrogen production from catalytic reforming of the aqueous fraction of pyrolysis bio-oil with modified Ni-Al catalysts. Int J Hydrogen Energy 2014;39:14642-52.

[46] Salehi E, Azad FS, Harding T, Abedi J. Production of hydrogen by steam reforming of bio-oil over $Ni/Al_2O_3$ catalysts: Effect of addition of promoter and preparation procedure. Fuel Process Technol 2011;92:2203-10.

[47] Seyedeyn-Azad F, Salehi E, Abedi J, Harding T. Biomass to hydrogen via catalytic steam reforming of bio-oil over Ni-supported alumina catalysts. Fuel Process Technol 2011;92:563-9.

[48] Fu P, Yi W, Li Z, et al. Investigation on hydrogen production by catalytic steam reforming of maize stalk fast pyrolysis bio-oil. Int J Hydrogen Energy 2014;39:13962-71.

[49] Czernik S, French R. Distributed production of hydrogen by auto-thermal reforming of fast pyrolysis bio-oil. Int J Hydrogen Energy 2014;39:744-50.

[50] Yan C, Cheng F, Hu R. Hydrogen production from catalytic steam reforming of bio-oil aqueous fraction over $Ni/CeO_2$-$ZrO_2$ catalysts. Int J Hydrogen Energy 2010;35:11693-9.

[51] Trimm DL. Coke formation and minimisation during steam reforming reactions. Catal Today 1997;37:233-8.

[52] Angeli SD, Pilitsis FG, Lemonidou AA. Methane steam reforming at low temperature: Effect of light alkanes' presence on coke formation. Catal Today 2014:119-28.

[53] Wu C, Williams PT. Investigation of coke formation on Ni-Mg-Al catalyst for hydrogen production from the catalytic steam pyrolysis-gasification of polypropylene. Appl Catal B 2010;96:198-207.

[54] Blanco PH, Wu C, Williams PT. Influence of $Ni/SiO_2$ catalyst preparation methods on hydrogen production from the pyrolysis/reforming of refuse derived fuel. Int J Hydrogen Energy 2014;39:5723-32.

[55] Barbarias I, Lopez G, Amutio M, et al. Steam reforming of plastic pyrolysis model hydrocarbons and catalyst deactivation. Appl Catal A 2016;527:152-60.

[56] Sánchez-Sánchez MC, Navarro RM, Fierro JLG. Ethanol steam reforming over $Ni/La$-$Al_2O_3$ catalysts: Influence of lanthanum loading. Catal Today 2007;129:336-45.

[57] Zhang L, Li W, Liu J, Guo C, Wang Y, Zhang J. Ethanol steam reforming reactions over $Al_2O_3 \cdot SiO_2$-supported Ni-La catalysts. Fuel 2009;88:511-8.

[58] He Z, Yang M, Wang X, Zhao Z, Duan A. Effect of the transition metal oxide supports on hydrogen production from bio-ethanol reforming. Catal Today 2012;194:2-8.

[59] Lin K, Wang C, Chien S. Catalytic performance of steam reforming of ethanol at low temperature over $LaNiO_3$ perovskite. Int J Hydrogen Energy 2013;38:3226-32.

[60] Vicente J, Montero C, Ereña J, Azkoiti MJ, Bilbao J, Gayubo AG. Coke deactivation of Ni and Co catalysts in ethanol steam reforming at mild temperatures in a fluidized bed reactor. Int J Hydrogen Energy 2014;39:12586-96.

[61] Montero C, Ochoa A, Castaño P, Bilbao J, Gayubo AG. Monitoring $Ni^0$ and coke evolution during the deactivation of a $Ni/La_2O_3$-$\alpha Al_2O_3$ catalyst in ethanol steam reforming in a fluidized bed. J Catal 2015;331:181-92.

[62] Vicente J, Ereña J, Montero C, Azkoiti MJ, Bilbao J, Gayubo AG. Reaction pathway for ethanol steam reforming on a $Ni/SiO_2$ catalyst including coke formation. Int J Hydrogen Energy 2014;39:18820-34.

[63] Wang Z, Pan Y, Dong T, et al. Production of hydrogen from catalytic steam reforming of bio-oil using C12A7-$O^-$-based catalysts. Appl Catal A 2007;320:24-34.

[64] Wu C, Huang Q, Sui M, Yan Y, Wang F. Hydrogen production via catalytic steam reforming of fast pyrolysis bio-oil in a two-stage fixed bed reactor system. Fuel Process Technol 2008;89:1306-16.

[65] Lan P, Xu Q, Zhou M, Lan L, Zhang S, Yan Y. Catalytic steam reforming of fast pyrolysis bio-oil in fixed bed and fluidized bed reactors. Chem Eng Technol 2010;33:2021-8.

[66] Cao J, Shi P, Zhao X, Wei X, Takarada T. Catalytic reforming of volatiles and nitrogen compounds from sewage sludge pyrolysis to clean hydrogen and synthetic gas over a nickel catalyst. Fuel Process Technol 2014;123:34-40.

[67] Shen Y, Chen M, Sun T, Jia J. Catalytic reforming of pyrolysis tar over metallic nickel nanoparticles embedded in pyrochar. Fuel 2015;159:570-9.

[68] Garcia L, French R, Czernik S, Chornet E. Catalytic steam reforming of bio-oils for the production of hydrogen: Effects of catalyst composition. Appl Catal A 2000;201:225-39.

[69] Lan P, Lan LH, Xie T, Liao AP. The preparation of syngas by the reforming of bio-oil in a fluidized-bed reactor. Energy Sources Part A 2014;36:242-9.

[70] Xie H, Yu Q, Zuo Z, Han Z, Yao X, Qin Q. Hydrogen production via sorption-enhanced catalytic steam reforming of bio-oil. Int J Hydrogen Energy 2016;41:2345-53.

[71] Medrano JA, Oliva M, Ruiz J, García L, Arauzo J. Hydrogen from aqueous fraction of biomass pyrolysis liquids by catalytic steam reforming in fluidized bed. Energy 2011;36:2215-24.

776 [72] Czernik S, French R, Feik C, Chornet E. Hydrogen by catalytic steam reforming of
777 liquid byproducts from biomass thermoconversion processes. Ind Eng Chem Res
778 2002;41:4209-15.

779 [73] Joensen F, Rostrup-Nielsen JR. Conversion of hydrocarbons and alcohols for fuel
780 cells. J Power Sources 2002;105:195-201.

781 [74] Li H, Xu Q, Xue H, Yan Y. Catalytic reforming of the aqueous phase derived from
782 fast-pyrolysis of biomass. Renew Energy 2009;34:2872-7.

783